

Morphology, Microstructure and Transport Properties of ZnO Decorated SiO₂ Nanoparticles

Joseph E. Van Nostrand*

Air Force Research Laboratory, Information Directorate, Rome, NY

Rebecca Cortez

Union College, Schenectady, NY

Zachary P. Rice, Nathaniel C. Cady, and Magnus Bergkvist

Albany College of Nanoscale Science & Engineering, Albany, NY

(Dated: April 15, 2010)

We report on a novel, surfactant free method to achieve nanocrystalline ZnO decoration of an SiO₂ nanoparticle at ambient temperature. The size distribution of the naked and decorated SiO₂ nanoparticles is measured by dynamic light scattering, and a monodisperse distribution is observed for each. The morphology and microstructure of the nanoparticles are explored using atomic force microscopy and high resolution transmission electron microscopy. Investigation of the optical properties of the ZnO decorated SiO₂ nanoparticles shows absorption at 350 nm. This blue shift in absorption compared to bulk ZnO is shown to be consistent with quantum confinement effects due to the small size of the ZnO nanocrystals. Finally, the electronic transport properties of the nanoparticles is explored by scanning conductance atomic force microscopy. A memristive hysteresis in the transport properties of the individual ZnO decorated SiO₂ nanoparticles is observed. Optical absorption measurements suggest the presence of oxygen vacancies, the migration and annihilation of which appears to contribute to the dynamic conduction properties of the ZnO decorated nanoparticles. We believe this to be the first demonstration of a ZnO decorated SiO₂ nanoparticle, and represents a simple yet powerful way of achieving the optical and electrical properties of ZnO combined with the simplicity of SiO₂ synthesis.

PACS numbers: 61.46.-w, 61.46.Hk, 66.10.Ed, 68.37.Ps, 68.37.Lp, 73.61.Ga, 78.67.Bf, 81.05.Dz, 81.07.-b

I. INTRODUCTION

One dimensional nanostructures such as nanowires, nanotubes, and nanoshells have received a great deal of interest because of their morphology-dependent physico-chemical properties and technological relevance in comparison to their bulk phase counterparts¹. Oxide materials have become a major focus in the emerging area of nanoelectronics, especially those categorized as wide bandgap. Potential applications include high speed/high power electronics², nano-crossbar computing³, optical emitters and detectors in the visible and ultraviolet^{4,5}, chemical and biological sensors⁶, and, recently, memristors⁷⁻⁹, which have been described as the fourth fundamental passive circuit element⁷. ZnO is a wide, direct bandgap semiconductor with a bandgap of 3.37 eV and unique photonic and electronic properties¹⁰. One dimensional ZnO nanometer size crystals not only have an enormous surface to volume ratio, but also exhibit significant size-dependent electronic and optical properties resulting from quantum confinement effects. Furthermore, ZnO nanomaterials show potential for excellent sensitivity and rapid response in nanoelectronic devices in comparison to larger size devices.

ZnO has wide applications in broad areas of photonics and electronics, and there has been considerable effort expended in attempting to control both the ZnO morphology and size on the nanometer scale^{10,11}. Techniques

such as physical vapor deposition on substrates patterned with noble metals which catalyze material from the vapor phase into the solid phase have been shown to produce single crystal wurtzite ZnO nanorods with controllable diameters¹¹. Wet chemical methods¹²⁻¹⁴ have also been employed for the synthesis of one dimensional ZnO nanostructures with high uniformity¹⁴. However, synthesis of nanometer size particles of single crystal ZnO which are approximately spherical in shape has proven difficult. For wet chemical techniques, this is believed to be due to the selective growth of the ZnO crystal planes resulting in uneven growth rates for the different crystallographic directions¹⁵. For vapor phase nanosynthesis techniques, the catalyst material is a stationary phase, and thus only high aspect ratio nanostructures can be achieved.

In this paper, we report on a novel technique for the synthesis of ZnO nanocrystals at ambient temperature that decorate an SiO₂ nanoparticle core. Previous efforts involving gold nanocluster decoration of silica nanoparticles have been reported by Westcott et. al¹⁶, however metal oxide nanocrystal synthesis on semiconductor oxide nanoparticles is an area yet to be fully explored. One advantage of this approach is that it enables wide bandgap engineering of oxides for novel memristive and photovoltaic nanostructures using a facile synthesis technique. The average diameter of the ZnO decorated SiO₂ nanoparticles was targeted to be 100 nm for the purposes of this study, however the nanoparticle size can

be reduced to a few tens of nanometers using the well established Stöber technique¹⁷. In addition, we have explored the optical absorption as well as the local electronic transport properties of individual nanoparticles. The measured optical and transport properties suggest the synthesis technique results in a high quality nanocrystalline ZnO coating the surface of the SiO₂ for use in low-dimensional physics studies as well as for applications in other nanoscale science and technology.

II. EXPERIMENT

The SiO₂ nanoparticles were synthesized using the Stöber method¹⁷, while the ZnO nanocrystals were synthesized using an ambient temperature hydrolytic method. After Stöber synthesis of the SiO₂ nanoparticles, the nanoparticles were washed by centrifugation at 13,300 rcf for 30 minutes. The supernatant was decanted off and replaced with an equal volume of ethanol, and the nanoparticles were resuspended. This washing process was repeated three times. In the hydrolytic ZnO synthesis method, a 1 ml suspension of SiO₂ nanoshells in ethanol was added to 10 ml of a 0.005 M solution of Zn(CH₃COO)₂·2H₂O (MW: 219.51 u) in ethanol and stirred at 350 RPM. To this mixture 520 μ l of NaOH (28-30%, Fisher Scientific) was added, and allowed to react for 24 hours at 30°C. As a control, the ZnO synthesis method was repeated without the presence of SiO₂ nanoparticles.

The resulting nanoparticles from each synthesis process were characterized by several methods as follows. Hydrodynamic radii were determined via dynamic light scattering (DLS) using a Zetasizer Nano (Malvern Instruments, UK). Room temperature bulk values for index of refraction and absorption were used for both the SiO₂ nanoparticles and ZnO decorated SiO₂ nanoparticles. Optical absorption measurements were performed using a Shimadzu UV-1800 spectrophotometer. Transmission electron microscopy measurements were performed using a JEOL 2010 and lacey carbon grids (Ted Pella, Redding, CA). Nanoparticle morphology and conductivity were measured using a Veeco Dimension V scanning probe microscope. Morphology measurements were performed in tapping mode using a Veeco RTESP probe, while electrical measurements were performed in contact mode using a Veeco OSCM-PT platinum coated tip. The SiO₂ nanoparticles and ZnO decorated nanoparticles were dispersed on a copper coated substrate for conductivity measurements in order to complete the circuit.

III. RESULTS AND DISCUSSION

A. Dynamic light scattering

Dynamic light scattering results for the different nanoparticles explored in this study are shown in Fig-

ure 1. Dynamic light scattering, also known as photon correlation spectroscopy, measures Brownian motion and relates this to the size of the particles being measured. An important feature of Brownian motion measured by DLS is that small particles move quickly in comparison to large particles, and the relationship between the size of a particle and its speed due to Brownian motion is defined in the Stokes-Einstein equation¹⁸. The fundamental size distribution determined by DLS is an intensity distribution. However, this can be converted to a volume distribution using Mie theory¹⁹, as is shown in Figure 1. The single peak in the DLS measurement suggest a monodisperse distribution for both the SiO₂ nanoparticles and the ZnO decorated SiO₂ nanoparticles. Based on a Gaussian fit to the DLS measurement results, the peak diameter for SiO₂ nanoparticles was determined to be 87 nm, while for ZnO decorated nanoparticles the diameter was 123 nm. This suggests an average ZnO “radius” of approximately 18 nm. Figure 1 also shows a gradual decrease in mean volume with increasing SiO₂ nanoparticle diameter. This may be due to the scattering measurement incorporating reflections from a small number of clusters of nanoparticles and interpreting this as a larger diameter SiO₂ single particle. This shoulder is not observed in the peak for the ZnO decorated nanoparticles, which suggests a lesser degree of clustering in solution by the ZnO decorated SiO₂ nanoparticles in comparison to the as grown SiO₂ nanoparticles. DLS measurements on the ZnO control nanoparticles (not shown), which were synthesized without the presence of SiO₂ nanoparticles, showed a significant degree of clustering. This clustering resulted in poor run to run correlation statistics, and thus prevented DLS measurement of the average diameter of the as grown ZnO control nanoparticles. As shown in Figure 1, the presence of SiO₂ nanoparticles during ZnO nanoparticle synthesis precludes ZnO cluster formation. This is probably due to the SiO₂ providing a surface for the ZnO nanoparticles to adhere to. This results in a significant improvement in control of the diameter of nanoparticles obtained using the synthesis method we describe in comparison to ZnO nanoparticles grown in a solution free of SiO₂ nanoparticles.

B. Morphological characterization by atomic force microscopy

An atomic force microscopy image showing morphology of SiO₂ nanoparticles synthesized using the Stöber method¹⁷ and dispersed on a silicon substrate is shown in Figure 2 (a). The image is 2 μ m \times 2 μ m, and the black to white grayscale is 40 nm. Individual nanoparticles can be clearly resolved, and the monodisperse distribution observed in Figure 2 (a) is consistent with the single peak in the DLS measurement shown in Figure 1. The SiO₂ nanoparticle diameter as determined by averaging the measured diameter of several SiO₂ nanoparticles chosen at random is consistent with the diameter of 87 nm

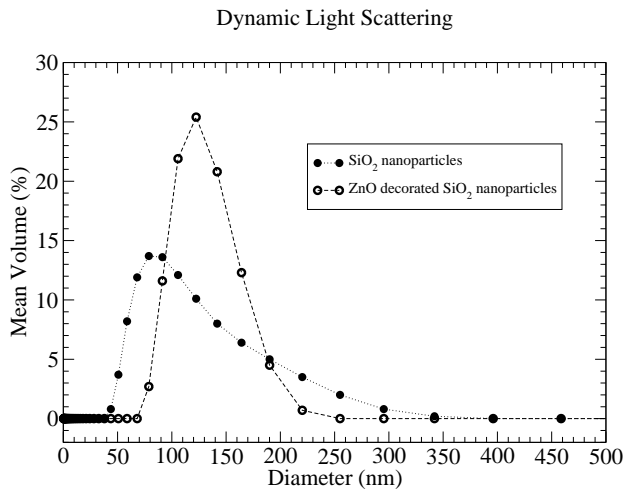


FIG. 1: Dynamic light scattering (DLS) measurement of volume diameter of SiO₂ and ZnO decorated SiO₂ nanoparticles. The single peak for both the SiO₂ and ZnO decorated nanoparticles suggests a monodisperse distribution for each dispersion. Based on a Gaussian fit to the DLS measurement results (not shown), the peak diameter for SiO₂ nanoparticles was 87 nm, while for ZnO decorated nanoparticles the diameter was 123 nm.

predicted by DLS to within one standard deviation. Figure 2 (b) is an atomic force microscopy image showing the morphology of ZnO decorated SiO₂ nanoparticles from the same lot of material shown in Figure 2 (a). The image is $2\ \mu\text{m} \times 2\ \mu\text{m}$, and the black to white grayscale is 250 nm. The ZnO coated nanoparticles show a greater degree of coalescence in comparison to the bare SiO₂ nanoparticles, which leads to the larger black to white grayscale for Figure 2 (b). The monodisperse distribution of ZnO coated nanoshells shown in Figure 1 by dynamic light scattering measurements suggests the process of agglomeration does not occur in solution, but rather may occur as the ethanol evaporates after the suspension of ZnO nanoshells is deposited on the silicon substrate.

C. Optical characterization by absorption spectroscopy

Results for room temperature optical absorption measurements of both the SiO₂ and ZnO decorated nanoparticles is shown in Figure 3. For the SiO₂ nanoparticles at least two absorption peaks can be identified. The higher energy peak near 225 nm is believed to be due to the E' center²⁰. Moreover, the shoulder in the SiO₂ spectra at 275 nm is in good agreement with the absorption attributed to intrinsic oxygen hole centers²¹, one of which is the non-bridging oxygen hole centers (NBOHC)^{22,23}. It should be noted that the absorption band near 600 nm associated with NBOHC is not observed in our SiO₂ nanoparticle samples. This result can be explained by the differences in oscillator strength, where the absorp-

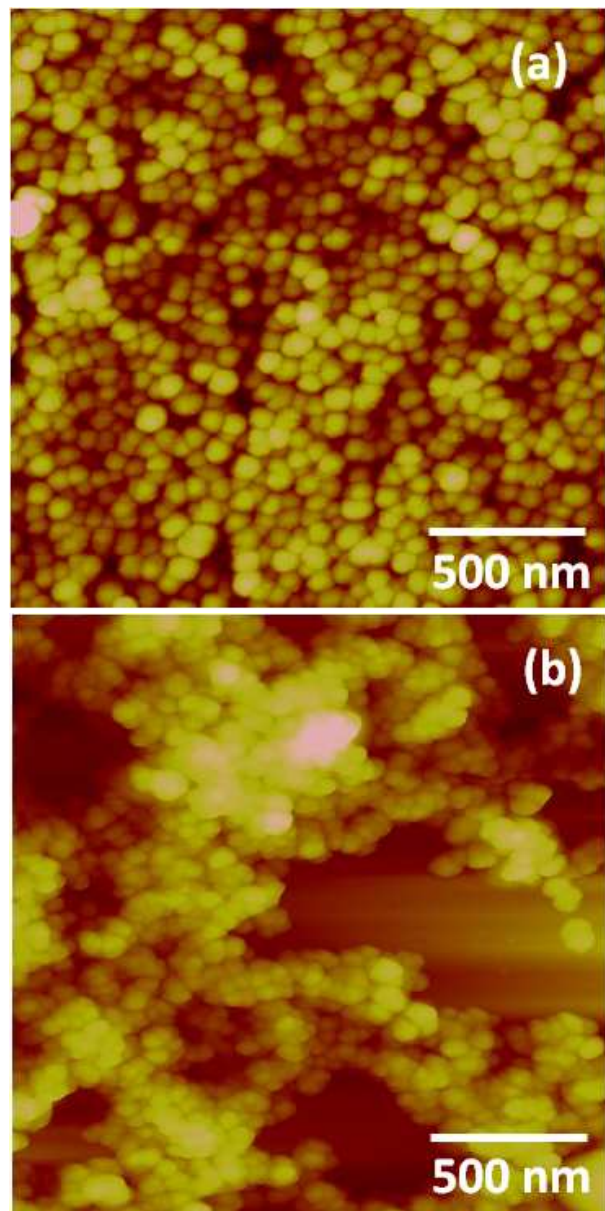


FIG. 2: Atomic force microscopy images showing morphology of (a) SiO₂ nanoparticles synthesized using the Stöber method¹⁷, and (b) ZnO decorated SiO₂ nanoparticles. Both images are $2\ \mu\text{m} \times 2\ \mu\text{m}$. The black to white grayscale is 40 nm in (a) and 250 nm in (b).

tion band amplitude near 600 nm is predicted to be over 100 times smaller than the absorption band at 275 nm²².

For the ZnO decorated SiO₂ nanoparticle absorption shown in Figure 3, the absorption peak at 350 nm is blue shifted from the bulk value of 387 nm¹⁵ observed in high quality single crystal ZnO. This blue shift of the reduced dimension ZnO nanocrystals in comparison to bulk materials is believed to be due to size effects, as widely reported in the literature^{24,25}. The absorption spectrum of nanocrystals with a diameter larger than approximately 15 nm show a well developed maximum near the onset

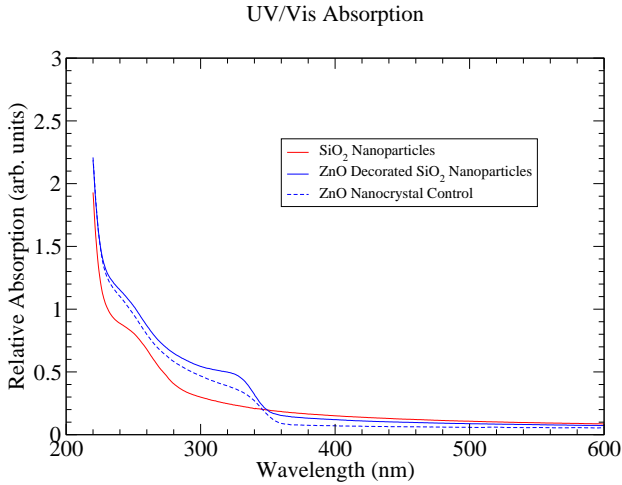


FIG. 3: Room temperature absorption spectrum of SiO_2 and ZnO decorated nanoparticles suspended in ethanol solution.

of absorption which is attributed to the first excitonic transition¹⁵. This excitonic transition is similarly observed in other direct bandgap II-VI material systems, such as CdS ²⁶. However, the first excitonic transition no longer appears in the absorption spectrum of smaller ZnO nanocrystals. Instead, other transitions are observed in the wavelength range 320 - 330 nm in the sub 15 nm size range. The shape of the crystallites, surface energy, and correlation effects will all influence the relative spacing of the energy levels²⁷, thus making the band structure source of the absorption difficult to clearly identify in this reduced size range. The optical absorption of ZnO nanocrystals synthesized as a control without the presence of SiO_2 nanoparticles is also shown in Figure 3. As can be seen in Figure 3, the absorption properties of the ZnO nanocrystals are nearly identical to those of the ZnO decorated SiO_2 nanoparticles, differing only in a slightly enhanced near bandedge absorption by the ZnO decorated nanoparticles compared to the ZnO nanocrystal control. The similarity in absorption properties between the ZnO nanocrystals and ZnO decorated SiO_2 nanoparticles suggests the SiO_2 nanoparticles do not interfere with the ZnO nanocrystal growth kinetics beyond providing a substrate for the ZnO nanocrystal interaction. No free ZnO nanocrystals are observed in solution when they are synthesized in the presence of SiO_2 nanoparticles. It is unclear at this point if the ZnO nanocrystals nucleate homogeneously in solution and then bind strongly to the SiO_2 surface, or if the SiO_2 nanoparticles provide a substrate for heterogeneous nucleation.

D. Microstructural analysis

Structural information about the SiO_2 and ZnO decorated nanoparticles is provided by the transmission electron diffraction analysis shown in Figure 4. As shown in Figure 4 (a), the SiO_2 is amorphous and is decorated

by small, 5-10 nm nanoparticles of crystalline ZnO. The high resolution transmission electron microscopy image in Figure 4 (b) shows the ZnO nanocrystals have coalesced, forming a porous, polycrystalline shell around the SiO_2 nanoparticle. The lattice fringes in the individual ZnO nanocrystals are clear and parallel within each nanocrystal. However, they are generally randomly oriented around the SiO_2 nanoparticle. This is consistent with the polycrystalline rings observed in the selected-area electron diffraction pattern (not shown) for the ZnO decorated SiO_2 nanoparticles. While the growth conditions we employ for synthesis of ZnO nanocrystals are similar to those previously reported^{28,29}, we believe this is the first demonstration of decorating an SiO_2 nanoparticle with a polycrystalline ZnO nanoparticles to control ZnO nanocrystal clustering. Use of SiO_2 nanoparticles as a substrate for ZnO nanocrystal attachment and subsequent growth also simplifies extraction of the ZnO nanocrystals from solution since they can easily be separated out using a benchtop ultracentrifuge. Since the SiO_2 nanoparticles synthesized using the Stöber method¹⁷ can be tailored to a range of sizes, it is possible to use this approach to produce ZnO decorated SiO_2 nanoparticles of the desired diameter without the need for elevated reaction temperatures. Further, the process enables the synthesis of larger diameter ZnO “shells” around SiO_2 nanoparticles without the use of surfactants which are often utilized to reduce the asymmetric growth rates encountered in fabrication of low dimensional ZnO shapes¹⁴. The diameter of ZnO nanocrystals in the 5-10 nm range is consistent with the blue shift observed in the absorption spectra of Figure 3.

E. Electronic transport characterization by scanning conductance spectroscopy

Figure 5 shows the measured transport properties of the ZnO decorated SiO_2 nanoparticles for consecutive positive then negative voltage sweeps as measured by a scanning conductance atomic force microscope. In each “pass” shown in Figure 5, the ZnO decorated nanoparticles were exposed to a forward bias from 0 to 5 volts and back to 0 (Figure 5 (a)), then a reverse bias from 0 to -5 volts and back to 0 (Figure 5 (b)). The hysteresis in the transport properties of the nanoparticles can be clearly observed. The mechanism for the change in resistance is not yet clear, but the presence of oxygen vacancies suggested in Figure 3 may be contributing to the dynamic conduction properties observed in Figure 5. The presence of oxygen vacancies in the ZnO nanocrystals would also be in agreement with the work of Szot et. al³⁰, whose work demonstrated that electrochemical migration of oxygen ions resulted in significant changes in oxide thin film conductivity.

Migration of ions in metal oxide films is believed to be the fundamental physical mechanism⁷ providing the basis for the exciting new area of “memristors.” A memristor is

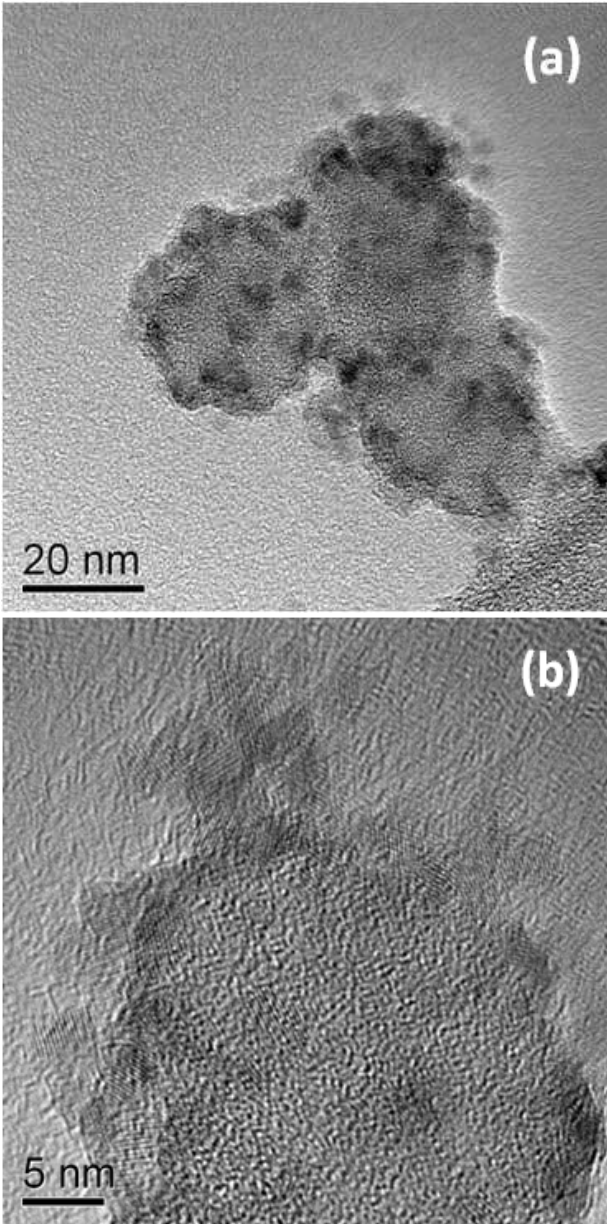


FIG. 4: (a) Transmission electron microscopy image of ZnO nanoshells with SiO₂ core decorated with coalesced ZnO nanocrystals. (b) High resolution electron micrograph showing amorphous SiO₂ core and lattice fringing of the polycrystalline layer of ZnO nanocrystals.

a two-terminal electronic device whose resistance can be precisely modulated by charge transport through the device. Memristors are typically fabricated by sandwiching an oxide material between two metal contacts. However, a lack of device repeatability has limited the technological implementation of memristors. Ions in the oxide material are subject to high electric fields, and their mobility is enhanced by localized Joule heating. Ions migrate and often form a “filament,” which subsequently provides a low resistance path through the oxide material³¹. An al-

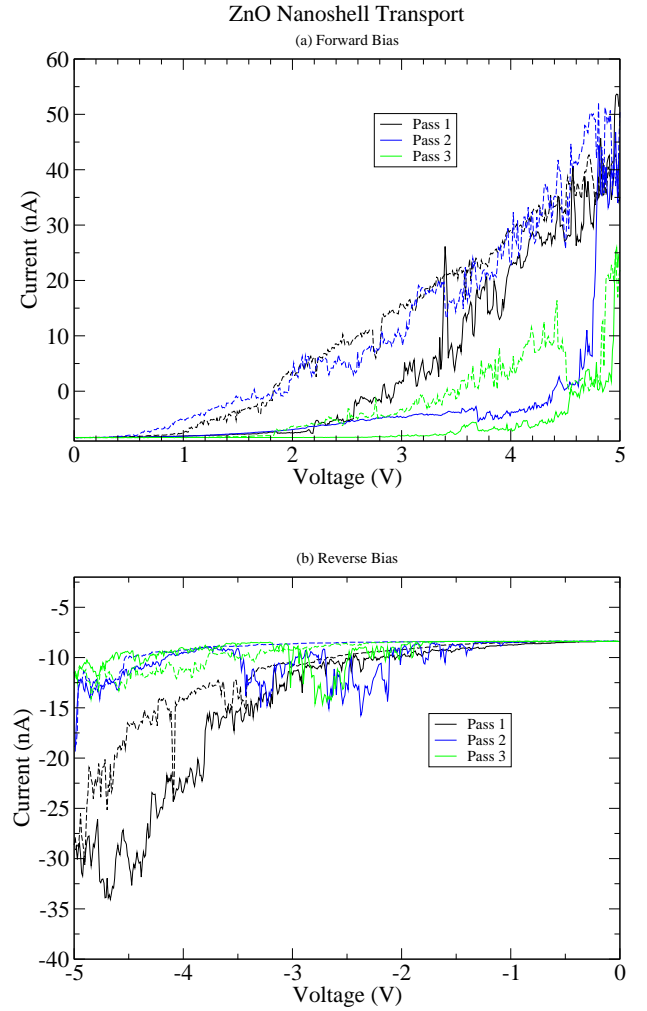


FIG. 5: Transport properties of ZnO decorated SiO₂ nanoparticles in the (a) forward, and (b) reverse bias directions as measured by scanning conductance atomic force microscope. Nanoparticles were alternately exposed to forward then reverse bias in each “pass.” In each pass shown, the ZnO decorated nanoparticles were exposed to a forward bias from 0 to 5 volts (solid line) and back (dashed line) to 0 (Figure 5 (a)), then a reverse bias from 0 to -5 volts and back to 0 (Figure 5 (b))

ternative mechanism for dynamic transport in TiO₂ thin films described by Yang et. al⁸ involves oxygen vacancies drifting towards the cathode forming localized conducting channels in the oxide, while, at the same time, O²⁻ ions drift towards the anode where they evolve out of the oxide layer as O₂ gas. Based on the results in Figure 5, it is not clear if there is any filament formation in the ZnO decorated SiO₂ nanoparticles as described by Waser³¹. As the number of passes increases, the overall resistivity of the ZnO decorated SiO₂ nanoparticle also increases. This may be due to a redistribution or possibly evolution of ions from the ZnO nanocrystal layer⁸. This trend of increasing resistivity of the oxide nanoparticle with each pass limits the viability of ZnO decorated

SiO₂ nanoparticles for memristor applications, but may prove useful in solar applications where a resistive nanomaterial with strong absorption in the ultraviolet is desirable for photoconductivity³². It is interesting to note that no current could be measured for the SiO₂ nanoparticles over the applied voltage range from zero to ± 10 volts. Based on this, we believe the conductivity properties demonstrated by the ZnO decorated SiO₂ nanoparticles is dominated by the ZnO nanocrystals.

IV. CONCLUSIONS

We have demonstrated a facile technique for ambient temperature synthesis of a polycrystalline layer of ZnO nanocrystals decorating an SiO₂ nanoparticle core which represents a simple yet powerful way of achieving the optical and electrical properties of ZnO with the simplicity of SiO₂ synthesis. Dynamic light scattering and atomic force microscopy measurements suggest a monodisperse distribution of nanoparticles, and absorption measurements show ZnO optical properties consistent with high quality low-dimensional ZnO nanocrystals. Optical prop-

erties also suggest the presence of oxygen vacancies, which appear to contribute to the memristive transport properties of the ZnO decorated SiO₂ nanoparticles as measured by scanning conductance atomic force microscopy. High resolution transmission electron microscopy shows an amorphous SiO₂ core and lattice fringing of the polycrystalline layer of ZnO nanocrystals, consistent with the optical and electrical transport properties observed for these nanoshells. We believe this layered approach to nanoparticle synthesis will have use in a number of different metal oxide systems, and could provide a general technique for producing metal oxide nanoparticles of a target dimension with optical and electronic transport properties similar to the single crystal.

Acknowledgments

RC would like to acknowledge the National Science Foundation for support of this effort (Grant No. EEC-0824341). The work of ZPR and JEVN was supported by the Air Force Office of Scientific Research (AFOSR PM Kitt Reinhardt).

-
- * Electronic address: Joseph.VanNostrand@rl.af.mil
- ¹ Y. Xia, P. Yang, Y. Sun, Y. Wu, B. Mayers, B. Gates, Y. Yin, F. Kim, and H. Yan, *Adv. Mater.* **15**, 353 (2003).
 - ² B. Bayraktaroglu, K. Leedy, and R. Neidhard, *IEEE Elec. Dev. Lett.* **30**, 946 (2009).
 - ³ G. Snider and R. Williams, *Nanotechnology* **18**, 035204 (2007).
 - ⁴ X. Wang, Z. Tian, T. Yu, H. Tian, J. Zhang, S. Yuan, X. Zhang, Z. Li, and Z. Zou, *Nanotechnology* **21**, 065703 (2010).
 - ⁵ J. Kim, J.-H. Yun, C. Kim, Y. Park, J. Woo, J. Park, J.-H. Lee, J. Yi, and C.-S. Han, *Nanotechnology* **21**, 115205 (2010).
 - ⁶ Y.-S. Huang, Y.-Y. Chen, and T.-T. Wu, *Nanotechnology* **21**, 009903 (2010).
 - ⁷ D. Strukov, G. Snider, D. Stewart, and R. Williams, *Nat. Lett.* **453**, 80 (2008).
 - ⁸ J. Yang, F. Miao, M. Pickett, D. Ohlberg, D. Stewart, C. Lau, and R. Williams, *Nanotechnology* **20**, 215201 (2009).
 - ⁹ A. Shih, W. Zhou, J. Qiu, H.-J. Yang, S. Chen, Z. Mi, and I. Shih, *Nanotechnology* **21**, 125201 (2010).
 - ¹⁰ F. Teherani and C. Litton, *SPIE Proceedings Zinc oxide materials and devices II*, vol. 6474 (2007).
 - ¹¹ Z. Wang, *J. Nanosci. Nanotechnol.* **8**, 27 (2008).
 - ¹² X. Cao, W. Ning, and L. Li, *Sensors Actuators B* **129**, 268 (2008).
 - ¹³ B. Liu and H. Zeng, *J. Am. Chem. Soc.* **125**, 4430 (2003).
 - ¹⁴ L. Guo, Y. Ji, and H. Xu, *J. Am. Chem. Soc.* **124**, 14864 (2002).
 - ¹⁵ X. Cao, N. Wang, and L. Wang, *Nanotechnology* **21**, 065603 (2010).
 - ¹⁶ S. Westcott, S. Oldenburg, T. Lee, and N. Halas, *Langmuir* **14**, 5396 (1998).
 - ¹⁷ W. Stöber, A. Fink, and E. Bohn, *J. Colloid Interface Sci.* **26**, 62 (1968).
 - ¹⁸ A. Kholodenko and J. Douglas, *Phys. Rev. E* **51**, 1081 (1995).
 - ¹⁹ M. Kerker, *The Scattering of Light and Other Electromagnetic Radiation* (Academic Press, New York, 1969).
 - ²⁰ R. Weeks and C. Nelson, *J. Appl. Phys.* **31**, 1555 (1960).
 - ²¹ S. Agnello and B. Boizot, *J. Non-Crystl. Sol.* **322**, 84 (2003).
 - ²² D. Griscom, *J. Ceram. Soc. Jpn.* **99**, 899 (1991).
 - ²³ L. Skuja and R. Silin, *Phys. Stat. Sol. (a)* **56**, 1 (1979).
 - ²⁴ L. Brus, *Appl. Phys.* **A53**, 465 (1991).
 - ²⁵ S. Oldenburg, R. Averitt, S. Westcott, and N. Halas, *Chem. Phys. Lett.* **288**, 243 (1998).
 - ²⁶ T. Vossmeier, L. Katsikas, M. Giersig, I. Popovic, K. Diesner, A. Chemseddine, A. Eychmüller, and H. Weller, *Chem. Phys. Lett.* **288**, 243 (1998).
 - ²⁷ A. Alivisatos, *J. Phys. Chem.* **100**, 13226 (1996).
 - ²⁸ L. Spanhel and M. Anderson, *J. Am. Chem. Soc.* **113**, 2826 (1991).
 - ²⁹ E. Meulenkamp, *J. Phys. Chem. B* **102**, 5566 (1998).
 - ³⁰ K. Szot, W. Speier, G. Bihlmayer, and R. Waser, *Nature Materials* **5**, 312 (2006).
 - ³¹ R. Waser, R. Dittmann, G. Staikov, and K. Szot, *Adv. Mater.* **21**, 2632 (2009).
 - ³² F. Krebs, Y. Thomann, R. Thomann, and J. Andreasen, *Nanotechnology* **19**, 424013 (2008).